Title
A processable, high-performance dielectric elastomer and multilayering process

Journal
Science, 377(6602)

ISSN
0036-8075

Authors
Shi, Ye
Askounis, Erin
Plamthottam, Roshan
et al.

Publication Date
2022-07-08

DOI
10.1126/science.abn0099

Peer reviewed

A Processable, High-performance Dielectric Elastomer and Multilayer Dielectric Elastomer Actuator

Ye Shi[1], Erin Askounis[1], Roshan Plamthottam[1], Tom Libby[2], Zihang Peng[1], Kareem Youssef[1], Junhong Pu[1], Ron Pelrine[2] & Qibing Pei[1,*]

1. Department of Materials Science and Engineering, University of California, Los Angeles, Los Angeles, CA, USA

2. SRI International, Menlo Park, CA, USA

* *qpei@seas.ucla.edu*

Abstract

Dielectric elastomer (DE) materials can act as deformable capacitors to generate mechanical work in response to an electric field. However, current widely used DEs are based on acrylic and silicone elastomers commercially manufactured for different purposes. Acrylic based DEs require prestretching to achieve high actuation strains and lack processing flexibility. Silicone based DEs allow for processability and rapid response, but produce much lower strains. A processable, high-performance dielectric elastomer (PHDE) with a bimodal network structure and hydrogen-bonding crosslinks is synthesized. The PHDE exhibits a maximum area strain of 190% and maintains strain

higher than 110% at 2 Hz, without prestretching. PHDE actuators also show high force and energy outputs, with a peak energy density of ~88 J/kg. Owing to processing flexibility, multilayer PHDE actuators are fabricated by a novel dry stacking process. These PHDE stacks maintain the high actuation performance of single layer films and open the door to new DE devices, such as spider actuators and multifunctional roll actuators. The PHDE achieved actuation strains comparable to that of the best highly prestretched acrylic elastomers, with fast response and high processability afforded by silicone elastomers, thus becoming a promising artificial muscle material for the fabrication of soft robots, haptic and wearable devices.

Introduction

Natural muscle is a unique material system that not only provides high energy density, but also can operate in a combination of modes with varying frequency, strains, and cycles when stimulated with an electric pulse. Dielectric elastomer (DE) materials have been widely investigated as an "artificial muscle" with large electrically induced actuation strain, high energy density, fast response speed, and mechanical compliancy, which reproduce or in some aspects exceed the multifunctional performance of natural muscles[1-9]. When a DE film is sandwiched between a pair of compliant electrodes, it acts as a deformable capacitor and is known as a dielectric elastomer actuator (DEA)[10]. When a voltage is applied, the electric field across the DE generates a strong electrostatic interaction between the electrodes, known as a Maxwell stress (p), which compresses the film in the thickness direction and expands it in area. The Maxwell

stress is described as:

$$p = \varepsilon_0 \varepsilon_r E^2 = \varepsilon_0 \varepsilon_r (V/z)^2 \qquad \text{Eq. 1}$$

where E is the electric field, ε_r is the dielectric constant of the DE material, ε_0 is the permittivity of vacuum, V is the applied voltage and z is the film thickness. The actuation strain S_z across the DE film is, considering a free boundary approximation:

$$S_z = -p/Y' = -\varepsilon_0 \varepsilon_r (V/z)^2 / Y' = \frac{1}{1+s_A} - 1 \qquad \text{Eq. 2}$$

where Y' is the apparent modulus of elasticity at the actuated strain and S_A is the area strain, assuming the DE polymer is incompressible in volume.

The electromechanical energy density (*e),* the amount of electrical energy converted to mechanical energy per unit volume of material for one cycle under constant field actuation, is often used to classify high strain, nonlinear materials. It is estimated as[1]:

$$e = -0.5 \; p \; ln(1 + s_z) = -0.5 \; (\varepsilon_r \varepsilon_0 E^2) \; ln(1 + s_z) \qquad \text{Eq. 3}$$

Based on the equations above, a high-performance DE material should have a proper stress-strain relationship, high stretchability, a large dielectric constant, and high dielectric strength.

Unfortunately, few DE materials can meet all these requirements and the selection of DE materials is also very limited[11,12]. Commercial 3M VHB™ acrylate adhesive tapes and silicone elastomer resins are the most widely used DE materials. However, VHB films suffer from low response speed and high viscoelastic losses while silicone elastomers tend to exhibit low maximum strains of 15-20% and low dielectric strength[4,13-15]. In addition, most of these soft conventional elastomers exhibit a long

stress-strain plateau[4,16] and their performance is limited by electromechanical instability (EMI)[10,17]. Under constant voltage, the electric field increases as the thickness of the DE decreases, resulting in progressively greater strain that proceeds until failure or induces unstable snap-through. EMI can be suppressed by applying a constant strain onto the DE film prior to actuation, known as a prestretching[18-20]. This, unfortunately, requires a rigid frame to maintain the applied strain, thus diminishing the compliancy of the overall actuators and eliminating a major benefit of soft artificial muscles. Prestretching can also lead to stress concentrations, rapid fatigue, and premature failure via crack propagation.

The processability of current DE materials leaves much to be desired. The development of multilayer DEAs that are able to output high force and energy at low voltages relies on the processability of DE thin films[6,21,22]. VHBs lack the processing flexibility for multilayer DEA fabrication as they are supplied as cured films and require a large degree of prestretching[23,24]. Silicone elastomers are more processable since they are available from various suppliers in uncured state. The commercially available stacked DEA based on silicone elastomers, the only one of its kind on the market, is offered by CTsystems in Switzerland, with a longitudinal strain of 3.3% which is well less than that of skeletal muscle (20%)[25]. While there have been advances in new DE materials, such as bottle-brush polymers[16,26], interpenetrating networked elastomers[27-29], and high dielectric constant silicone elastomers[30-34], DE materials that combine the processability and fast response of silicone elastomers with the high strain and work density of acrylic elastomers are still needed by the field. Such materials would open

the door to many applications for the DEAs, such as multilayer actuators for compliant motors and soft robotic assemblies.

We synthesized a new dielectric elastomer comprising of a bimodal network by using two difunctional acrylate crosslinkers with different chain lengths. The bimodal network enables a rapid increase in modulus at strains higher than 100%, thus suppressing runaway dielectric breakdown and EMI (Fig. 1a). We also introduced a small degree of hydrogen bonding in the network as weak physical crosslinks to efficiently reduce the viscoelasticity. The resulting processable high-performance dielectric elastomer (PHDE) shows large-strain, high energy output and fast actuation. The processability also allows a new dry stacking technique leading to stacked actuators producing comparably large strains as single films.

Results and Discussion

The new dielectric elastomer films with a bimodal network structure were fabricated via solution processing for high-performance actuation. The long chain segment in the bimodal network structure ensures large elongation and the second relatively short chain segment raises the modulus at modest strains to resist the rapid increases in Maxwell stress during actuation and suppress EMI (Fig. 1a)[18,35]. Compared to non-prestretched VHB, the elongation of bimodal networked elastomers is smaller because of their high crosslinking density, which leads to restricted chain mobility and fracture at low elongations. Fig. 1b shows the molecular structures of reactants we used to build our bimodal networked DE. Detailed formulations and nomenclature of

samples can be found in Table 1 in Supplementary Information. Butyl acrylate (BA) and isobornyl acrylate (IBOA) were selected as co-monomers to lower the modulus and improve the toughness of co-polymers, respectively. CN9021, an urethane diacrylate (UDA) with a high molecular weight (Supplementary Fig. 1), was selected as the flexible long-chain crosslinker and propoxylated neopentyl glycol diacrylate (PNPDA) was used as the short-chain crosslinker. Compared to previously explored short-chain crosslinkers such as hexanediol diacrylate, PNPDA has a softer and more extended chain which provides greater flexibility for fine tuning of the mechanical properties (Supplementary Fig. 2 and 3)[18]. 2,2-dimethoxy-2-phenylacetophenone (DMPA) and benzophenone (BP) were used as co-photoinitiators to ensure complete curing of the thin films. All the reactants were mixed into one solution and the films were directly processed from a liquid formulation and cured via exposure to ultraviolet light.

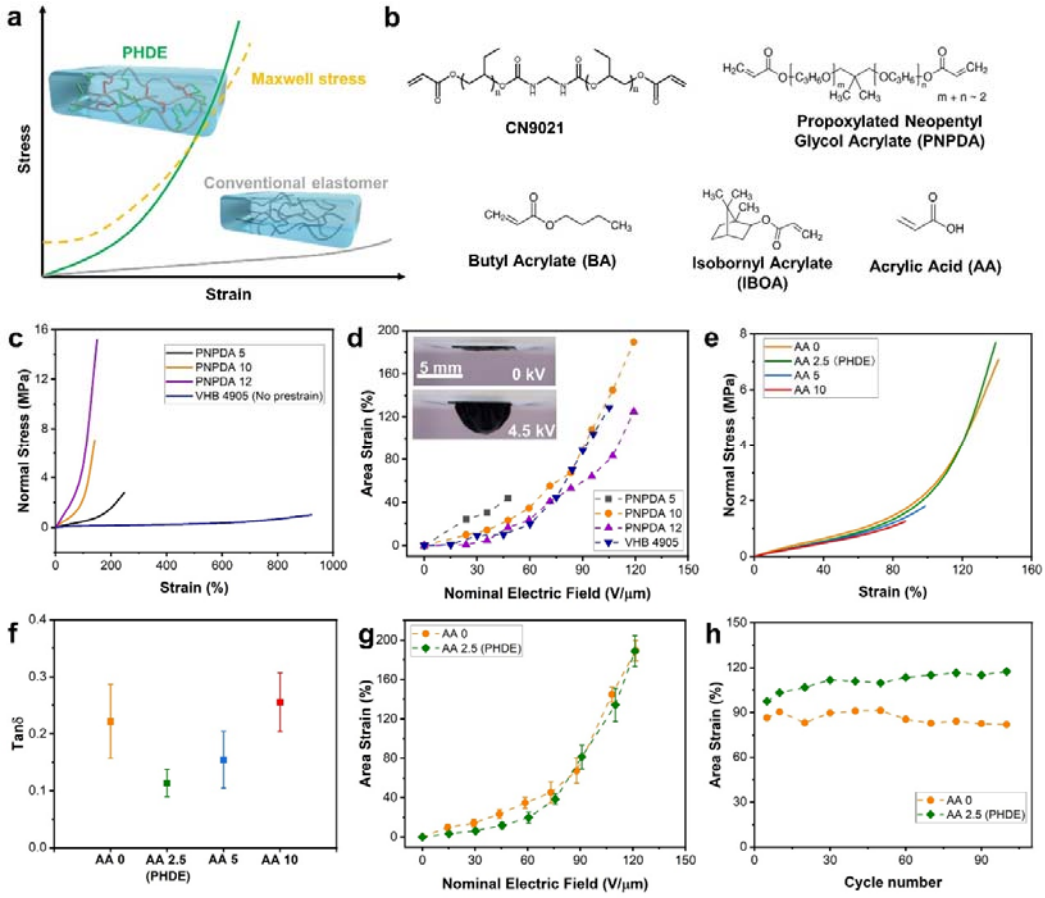

Fig. 1. Synthesizing bimodal networked DEs with a small amount of hydrogen bonds for high-performance actuation: (a) Schematic illustration of the design rules for DE with bimodal network structure. (b) Molecular structures of acrylates and diacrylates used for synthesis of bimodal networked DE. (c) Stress-strain relationships of bimodal DE materials with different concentrations (wt%) of PNPDA and VHB 4905 without prestrain. (d) Static actuation of bimodal DE materials with different concentrations of PNPDA and VHB 4905 with 300% biaxial prestrain, measured on a diaphragm. Carbon grease was used as the compliant electrodes. The inset shows photos of PNPDA 10 before and after being actuated. The film thickness is ~49 μm. (e) Stress-strain relationships of bimodal DE materials with different amounts (parts by weight) of AA.

(f) Mechanical loss factors (tanδ) of bimodal DE materials with different amounts of AA at room temperature. (g) Static actuation of bimodal DE without AA and PHDE (AA 2.5), measured on a diaphragm. (h) Cyclic actuation of bimodal DE without AA and PHDE (AA 2.5) under a 2 Hz square wave voltage for 100 cycles.

The mechanical properties of DEs were finely tuned by changing the concentrations of the short-chain crosslinker (PNPDA) and the co-monomer (BA). The total concentration (wt%) of PNPDA and BA was fixed and the stress-strain relationship was controlled by tuning the ratio between them[18]. As shown in Fig. 1c, as the concentration of PNPDA increases, the modulus increases and the stretchability decreases due to higher crosslinking density. Compared to non-prestretched VHB with a long stress-strain plateau[4,16], our DE materials with a bimodal network structure stiffen after a critical stretch ratio. The elastic modulus of the elastomer increases significantly after a critical stretching point as the noncrystallizable elastomer is driven into its non-Gaussian region and starts to have stress redistribution[36]. This critical stretch ratio shifts to a smaller value and the stiffening becomes more significant as the crosslink density increases. A moderate crosslinking density should be selected for high-performance actuation because the low modulus at small stretch ratios enables a higher actuation strain. As the stretch ratio increases during actuation, the DE will subsequently stiffen at the critical stretch ratio thus suppressing EMI and improve its actuation stability.

To find the optimized stress-strain relationship for actuation, we fabricated DEAs

using elastomers with different PNPDA concentrations and tested their static actuation performance in a diaphragm configuration (Fig. 1d)[37]. The elastomer films with carbon grease electrodes were mounted on a chamber with a circular cutout aligned with DEA's active area. We applied a small air pressure of ~0.33 kPa within the diaphragm chamber to bias the actuation out of plane in a dome shape. A digital camcorder was used to record the actuation process under an applied voltage and the strain was calculated based on the captured video. When 5 wt% of PNPDA was used, the DE performed poorly with highest actuation area strain of 43% at a driving voltage of 1.5 kV. This premature actuation failure is indicative of insufficient short-chain segments in the bimodal elastomer network. In contrast, the DE with 12 wt% of PNPDA shows a greater stiffening effect and its maximum strain was limited to 124% area strain. The DE with 10 wt% of PNPDA exhibits the best actuation performance with a maximum strain of 189% (Inset in Fig. 1d). No snap-through was observed during its actuation, indicating that EMI was fully suppressed without prestretching, which is also confirmed by modeling studies (Supplementary Fig. 4). This DE film also shows high dielectric strength as its apparent electrical breakdown field, which is defined by the voltage applied divided by the thickness at the maximum strain, reaches as high as 330 V/μm. This non-prestretched DE exceeds the performance of VHB 4905 with 300% biaxial prestrain in terms of both maximum strain and dielectric strength. The results demonstrated that the stress-strain relationship of DE with 10 wt% of PNPDA is ideal for PHDE fabrication.

The dielectric elastomers with tuned bimodal network structure successfully

suppress EMI without prestretching and deliver high actuation strain. Co-monomer of acrylic acid (AA) was further introduced in the DE network to modify the viscoelasticity and thus the response speed of the new DE. Hydrogen bonding is widely used in soft polymers such as polyurethanes and Nylons to enhance elasticity. AA provides side groups to form two-point hydrogen bonded dimers with themselves, as well as with the –NH- and –CH_2-O- groups on the CN9021 and PNPDA crosslinkers[38-40]. The stress-strain relationships and mechanical loss factors (tanδ) of DE materials with different amounts of AA added were compared in Fig. 1e and 1f, respectively. When a small amount of AA (2.5 parts of weight) is added, the stress-strain curve of DE is almost non-changed and the strain stiffening effect is preserved as indicated by the elastic modulus at different strain levels (Supplementary Table 2). The modified material shows similar mechanical properties including tensile strength (7.7 MPa), storage modulus (2.12 MPa) and elongation at break (139%) to those of DE without AA. The results indicate that the bimodal network and desired mechanical properties for high-strain actuation are well maintained after the small amount of AA is added. The formation of low-concentration hydrogen bonds compensates the decrease of covalent crosslinks and maintains the elasticity and modulus of DE. At the same time, the mechanical loss factor of DE, a measurement of the viscoelasticity, is decreased from ~0.22 to ~0.11 at room temperature and low frequencies. However, when the frequency is above 20 Hz, the storage modulus and loss factor of PHDE increases rapidly (Supplementary Fig. 5). As a comparison, non-prestretched VHB4905 has a loss factor as high as 0.64 at room temperature and low frequencies. Compared to the

covalent bonds, the hydrogen bonds formed by AA act as weak, physical crosslinks and can dynamically dissociate, leading to higher chain mobility in the network[41], which is further demonstrated by the lower glass transition temperature (T_g) of DE with AA (Supplementary Fig. 6). As more AA (5 and 10 parts of weight) is added, hydrogen bonds become highly concentrated in the DE network and the overall covalent crosslinking density (from both long-chain and short-chain crosslinkers) decreases. As a result, the elongation at break of DE decreases significantly and the loss factor increases again, resulting in inhibited actuation performance (Supplementary Fig. 7). Thus, the DE with 10 wt% of PNPDA and an additional 2.5 parts of AA is finalized as the PHDE composition for film preparation and device fabrication.

In order to characterize the actuation performance of these optimized PHDE films, we conducted a series of actuation tests of DE films with and without AA (Fig. 1g). PHDE reaches high maximum actuation strain of ~190% at a similar electric field. The leakage current is also maintained low after AA is added (Supplementary Fig. 8). More importantly, owing to lowered viscoelasticity, PHDE is able to provide higher actuation strain at high actuation speed. The DE films are actuated under a square wave voltage input with frequency of 2 Hz. The PHDE exhibits an average actuation of 110% area strain over 100 cycles, whereas the DE without AA only has an average of 70% strain (Fig. 1h and Supplementary Movie 1). In addition, the dielectric constant of PHDE was measured to be 5.35 at 1k Hz, higher than that of prestretched VHB4905, which is 3.47 (Supplementary Fig. 9).

The ability to outcouple force and perform usable work is an important feature of

DE materials. To measure the force output of the PHDE, we tested the film in a pure-shear mode which can be easily implemented on single layer films[37,42-44]. The set-up is shown in Fig. 2a. The single layer PHDE film measured 6 cm by 1 cm by 40 μm and the mass of the active material was ~0.030 g. The samples were preloaded under isometric conditions and the block force was monitored using a force gauge when voltages were applied across the film. As shown in Fig. 2b, when 0.6 N pre-load was applied, the block force exceeded 0.6 N at 2.5 kV and the film buckled. When 1.2 N pre-load was applied, the PHDE films produced ~0.95 N force at 2.5 kV and buckled at 3.0 kV, indicative that the block force was >1.2 N at 3.0 kV. When 1.4 N pre-load was used, the PHDE films reached a force output of ~1.2 N at 2.5 kV. However, due to the prestrain induced by the 1.4 N pre-load, the PHDE films were susceptible to break down at 3 kV. Thus the single layer PHDE in pure-shear mode was able to output a stable force of ~0.95 N (~0.40 MPa stress) at 2.5 kV with a 1.2 N pre-load. Compared to other DE devices with high force output[45], the high force of the PHDE was achieved without any prestretching mechanisms which would add significant extra weight and volume. We further evaluated the force output of single layer PHDE films at different frequencies, as shown in Fig. 2c. With a pre-load of 1.2 N and driving voltage of 2.5 kV, the force decreased to ~0.67 N (29% reduction) at 2 Hz and ~0.4 N at 20 Hz.

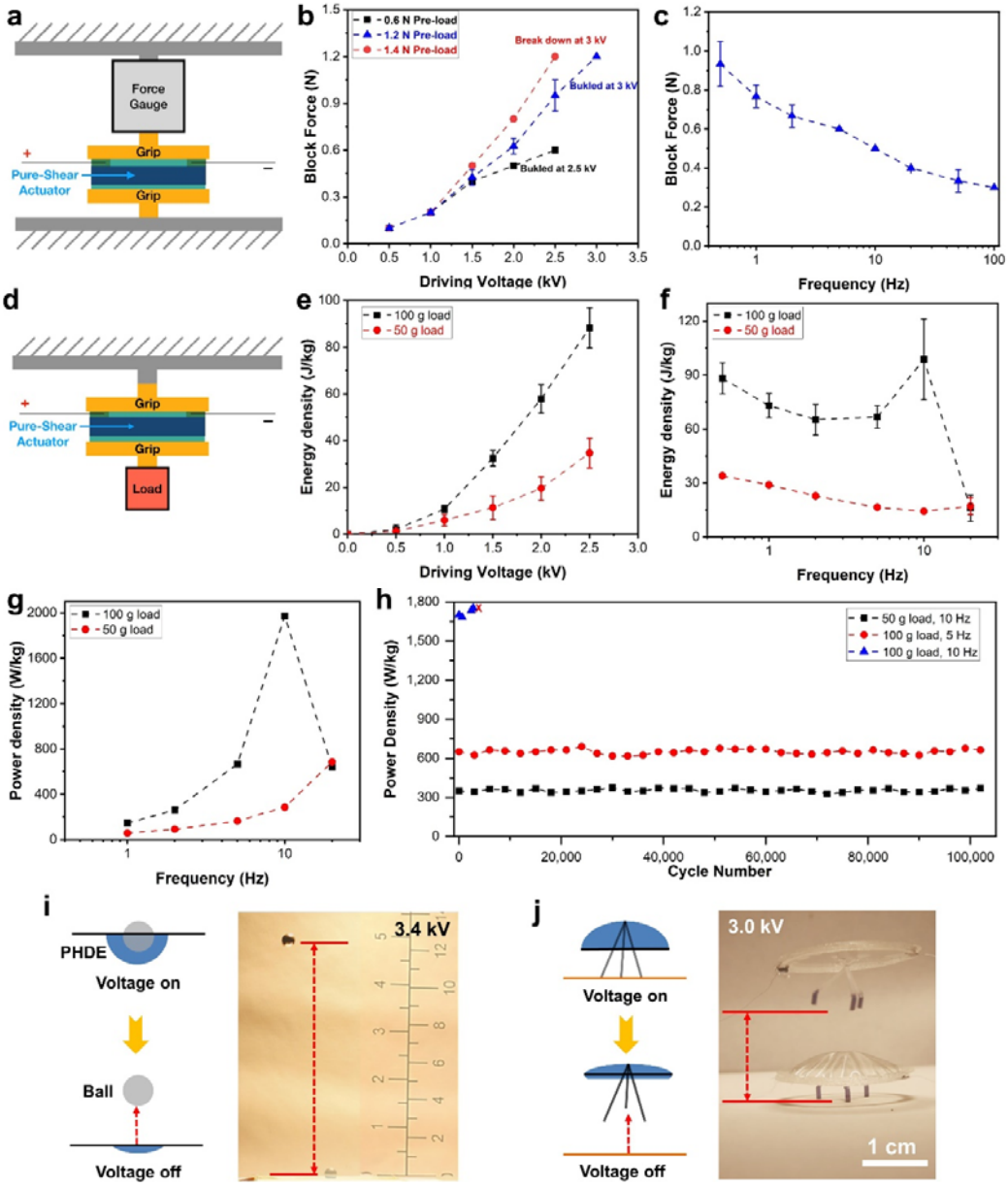

Fig. 2. Block force, energy density and power density properties of PHDE: (a) Schematic illustration of block force measurement setup (active area is 6 cm by 1 cm). (b) Block force of single layer PHDE films (40 μm thickness) under specified pre-loads. (c) Block force of single layer PHDE films at different frequencies. The driving voltage is 2.5 kV and the pre-load is 1.2 N. (d) Schematic illustration of the energy density measurement setup. (e) Energy density of single layer PHDE films measured at

specified loads. (f) Energy density at different frequencies. The driving voltage is 2.5 kV. (g) Average power density of single layer PHDE tested in pure-shear mode with different loads. (h) Life time tests on single layer PHDE films at different power outputs. (i) Ball toss by the PHDE actuator. (j) A jumping robot fabricated with a PHDE actuator.

The usable energy density of PHDE was evaluated by testing single layer films in pure-shear mode under isotonic conditions (Fig. 2d). As shown in Fig. 2e, the single layer PHDE films performed a specific work of ~35 J/kg during contraction at 2.5 kV with a 50 g load. With a 100 g load, the PHDE films were able to perform a specific work of ~88 J/kg at 2.5 kV (Supplementary Movie 2). The maximum driving voltage was lower than 3 kV because PHDE film was pre-stretched under heavy loads and its initial thickness was reduced. This energy density is more than twice than that of natural muscles (0.4 to 40 J/kg)[6]. We further measured the energy density of single layer PHDE films at various frequencies (Fig. 2f and Supplementary Movie 2). With 100 g load, the PHDE films maintained energy densities of ~65 J/kg at 2 Hz and ~16 J/kg at 20 Hz. At frequencies greater than or equal to 50 Hz, the films showed negligible linear strain, which indicated that the actuator was not able to effectively perform work at these frequencies. The peak energy density of ~99 J/kg at 10 Hz was caused by resonant responses of planar actuator systems[43,46]. Similarly, the PHDE films also showed a peak energy density at 20 Hz with 50 g load due to resonance. The PHDE films with 50 g load maintained energy densities of ~23 J/kg and ~17 J/kg at 2 Hz and 20 Hz, respectively. It should be pointed out that the block force and energy density can be also

tuned by adjusting the concentration of short chain crosslinker in the bimodal network to meet the requirements of different applications (Supplementary Fig. S10 and S11).

Based on the results of energy density measurements, we calculated the power densities of single layer PHDE films according to the average power outputs during contraction of PHDE films in the pure-shear mode (Fig. 2g)[43]. They showed high average power densities of ~670 W/kg at 5 Hz, 1970 W/kg at 10 Hz, and ~640 W/kg at 20 Hz with 100 g load. These power densities are about one order of magnitude higher than natural muscles[47]. In addition, the PHDE exhibited high stability when performing work. As shown in Fig. 2h, at 5 Hz with 100 g load, the PHDE film maintained the power density of ~660 W/kg after 100,000 cycles. At 10 Hz with 50 g load, the film also maintained a power density of ~350 W/kg for 100,000 cycles. The films were still functional after these tests. When performing a significant power at resonance (10 Hz and 100 g load), the life time of PHDE decreased to ~2800 cycles.

With large actuation strain, high energy density and fast response speed, PHDE could perform jobs which can be hardly achieved by other DE materials. We designed two of these applications to show the high performance of PHDE. The PHDE was first used to toss an aluminum ball weighing 91 mg, which is 20 times that of the PHDE film. The ball was placed on the actuator with 0.8 cm diameter. It sank into a hollow diaphragm as the film actuated, when the voltage turned off, the actuator snapped back, transferring the stored elastic energy to release the ball into the air. The high response speed ensured energy coupling efficiency during this process. The ball was thrown to a height of 12.1 cm (Fig. 2i and Supplementary Movie 3). The aluminum ball reached a

maximum potential energy of 0.1 mJ, which is ~10% of the actuation energy calculated in the PHDE film (Supplementary Fig. 12). Improved mechanical coupling and reduced viscoelasticity may increase the energy transfer efficiency and achieve a greater tossing height. Secondly, a miniature jumping robot using a single layer PHDE actuator was shown to achieve a height of 1.2 cm, which was ~67% of the theoretical height of this jumping system (Fig. 2j and Supplementary Movie 4). The 2 cm diameter PHDE actuator was seamlessly incorporated into a robotic framework and demonstrates its capacity as a light-weight, energy-dense actuator as the entire robot weighed less than 165 mg (Supplementary Fig. 13).

The PHDE's compatibility with conventional solution processing techniques and high actuation performance without prestretching enables high processing flexibility. We developed a dry stacking method and fabricated multilayer PHDE actuators. As illustrated in Fig. 3a, to fabricate an N-layer PHDE stack, N-1 PHDE thin films are casted on glass substrates and 1 film is prepared on PET. The blade coated films have a uniform thickness of ~40 μm. CNT electrodes and a thin layer of uncured acrylic polymer precursor acting as a binding layer are sprayed on the glass/PHDE films. To start the stacking, the PET/PHDE is aligned onto a glass/PHDE/CNT/precursor and laminated in a vacuum laminator. After UV curing the precursor layer, the glass is removed and the 2-layer PHDE stack which stays on PET is aligned onto another glass/PHDE/CNT/precursor to add the third PHDE layer. These processes are repeated until an N-layer PHDE stack is fabricated. Fig. 3b shows the pictures of a 10-layer PHDE stack with an array of 20 actuators. The cross-section of a PHDE stack was

examined by scanning electron microscopy (SEM) and the images in Fig. 3c show uniform thickness of PHDE layers and solid sealing between layers with the help of the thin binding layer.

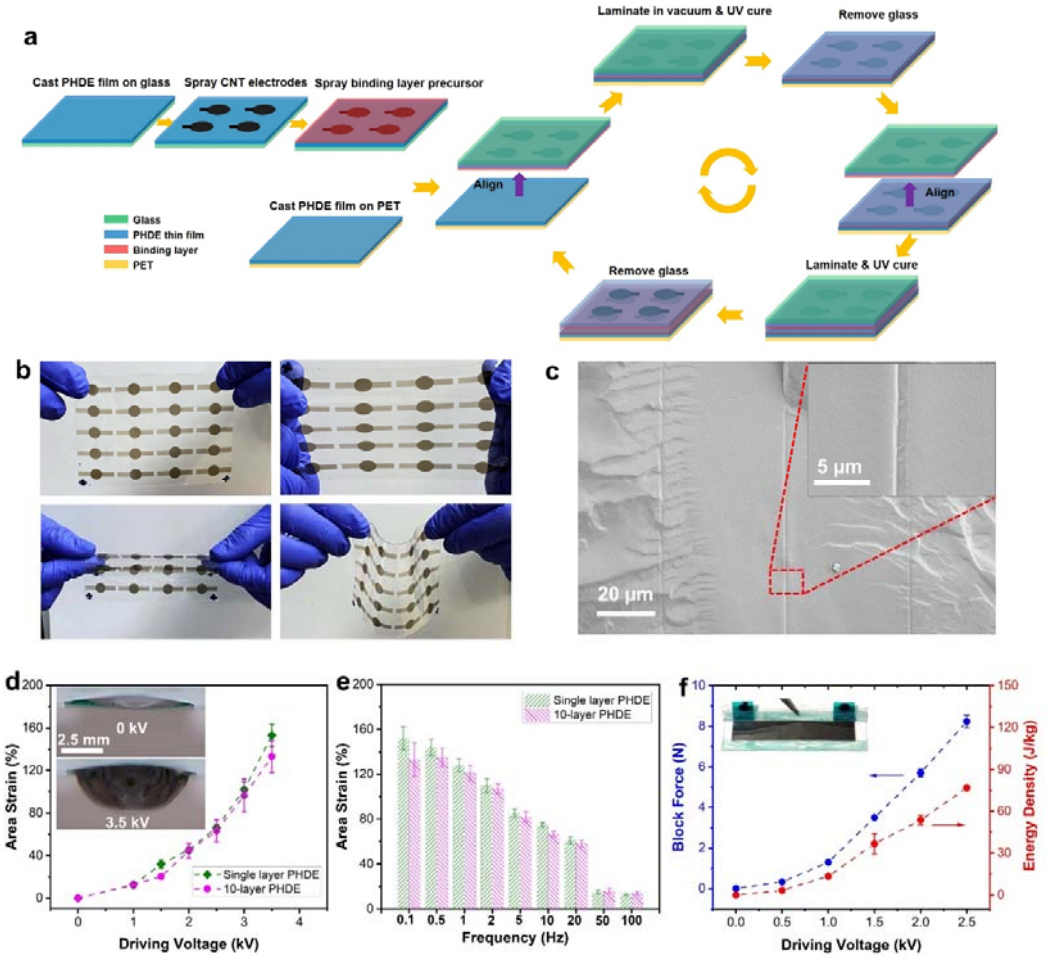

Fig. 3. Multilayer PHDE actuators enabled by a novel dry stacking method: (a) Diagram of "dry stacking" for multilayer PHDE actuator fabrication. (b) Photos of a 4" by 5" 10-layer PHDE stack with 20 actuators. (c) SEM images of cross-section view of a PHDE stack. The inset shows the thin binding layer between PHDE layers (the CNT layer is too thin to be identified at the interface). (d) Static actuation of single layer and 10-layer PHDE films, tested on a diaphragm. The photos show the 10-layer PHDE actuator before and after being actuated. CNT was used as compliant electrodes. (e)

Frequency response of single layer and 10-layer PHDE actuators under 3.5 kV (square wave, 50% duty cycle). (f) Block force and energy density of 10-layer PHDE stacks tested in pure-shear mode. The inset shows the photo of a 10-layer PHDE stack in pure-shear mode.

Compared to traditional "wet stacking" methods, which cure DE layers and apply electrodes in a layer-by-layer process[6,21,22,48], our dry stacking method for PHDE shows several advantageous features. It is compatible with large-scale materials processing with DE films prepared by blade coating, slot die coating or even roll-to-roll fabrication and the film thickness can be easily tuned (Supplementary Fig. 14). Additionally, this method minimizes defects and non-uniformity by screening cured single layers before stacking, thus achieving a good yield (Supplementary Fig. 15). The processing efficiency is greatly improved as large-area and numerous PHDE films with electrodes can be prepared at the same time before stacking. Another important feature that improves the efficiency of "dry stacking" is that it can be applied to PHDE stacks. For example, 10-layer PHDE stacks show high mechanical robustness and can be stacked together by "dry stacking" to form tens of layers of stacks (Supplementary Fig. 16).

The multilayer PHDE actuators maintain decent actuation performance compared to that of single layer PHDE actuators. Fig. 3d compares the static actuation performance of 10-layer and single layer PHDE actuators. Note that carbon nanotube (CNT) was used as compliant electrodes for both actuators, and the lower maximum strain compared to that of actuators with carbon grease electrodes could be caused by

decreased conductivity of CNT electrodes at highly stretched states. The actuation strain of 10-layer PHDE actuators is comparable to that of single layer actuators at the same low driving voltages. The strain is slightly lower at higher voltages, possibly due to greater bending stiffness at the non-active border around the 10-layer actuators (Supplementary Movie 5). Moreover, the multilayer actuator showed comparable response speed to single layer films. Both single layer and 10-layer PHDE actuators can reach strains above 110% at 2 Hz and maintain strains of ~60% at 20 Hz (Fig. 3e). The limited performance at frequencies higher than 50 Hz is caused by the viscoelastic loss of PHDE. This could possibly be reduced by introducing flexible side chains in the bimodal network to fill the space around the networked chains and lubricate their motion[16,17], or adding proper amounts of plasticizers as lubricants in the network to promote the chain mobility[18]. Fig. 3f shows block force and energy density of 10-layer PHDE stacks tested in pure-shear mode with the same planar dimension as single layer ones. At 2.5 kV, 10-layer PHDE stacks perform ~8.2 N force under a 12 N pre-load and ~77 J/kg work density with a 1000 g load. They maintain high forces (~6.7 N at 2 Hz and ~5.3 N at 20 Hz) and energy densities (~48 J/kg at 2 Hz and ~13 J/kg at 20 Hz) at high frequencies, thus being able to deliver high power (Supplementary Fig. 17). The small performance reduction when compared to single layer films may be attributed to (1) the presence of binding layers that can lower the stacking efficiency and (2) there may have been variation of actuation performances among the individual PHDE layers in the stack.

The development of “dry stacking” fabrication method, along with the tunability

and processability of the PHDE, opens the door to new possibilities with DE device fabrication. As an example, we fabricated "Spider" actuators, which couple radial strain to linear movement while maintaining highly uniform load distribution (Figure 4a). Spider actuators were previously identified as a potential DEA design[49], but never characterized, in part because they are not compatible with films that require high prestretching. The basic concept uses radially symmetric inclined "legs" to couple axial force to radial loading of a circle of DE film. The angle of the legs relative to the film changes during actuation, giving the linkage nonlinear mechanical advantage that can be tuned to maximize performance. We built one instantiation of this linkage, tuned for high axial force, and tested it with 4-layer PHDE stacks with an active area of ~4.8 cm^2. PHDE stacks facilitated the fabrication because these relatively stiff free-standing films were easy to handle. As shown in Fig. 4b and Supplementary Movie 6, we demonstrated a PHDE based spider actuator which successfully lifted a 200 g load with ~3.0 mm linear displacement at 2.5 kV. The specific work based on the mass of active PHDE was calculated to be ~74 J/kg. Under a gravitational load, the actuator work is limited by the nonlinear properties of the linkage: beyond a critical strain, the spring ratio of this structure becomes negative and the structure can collapse (Supplementary Movie 6). Physical stops that limit actuation below this critical point could maximize performance without unstable behavior. One of the main benefits of this type of architecture is that it can dramatically increase the overall stroke of the actuator. Spider structures can theoretically be stacked in series to produce high force and very high displacement actuator systems.

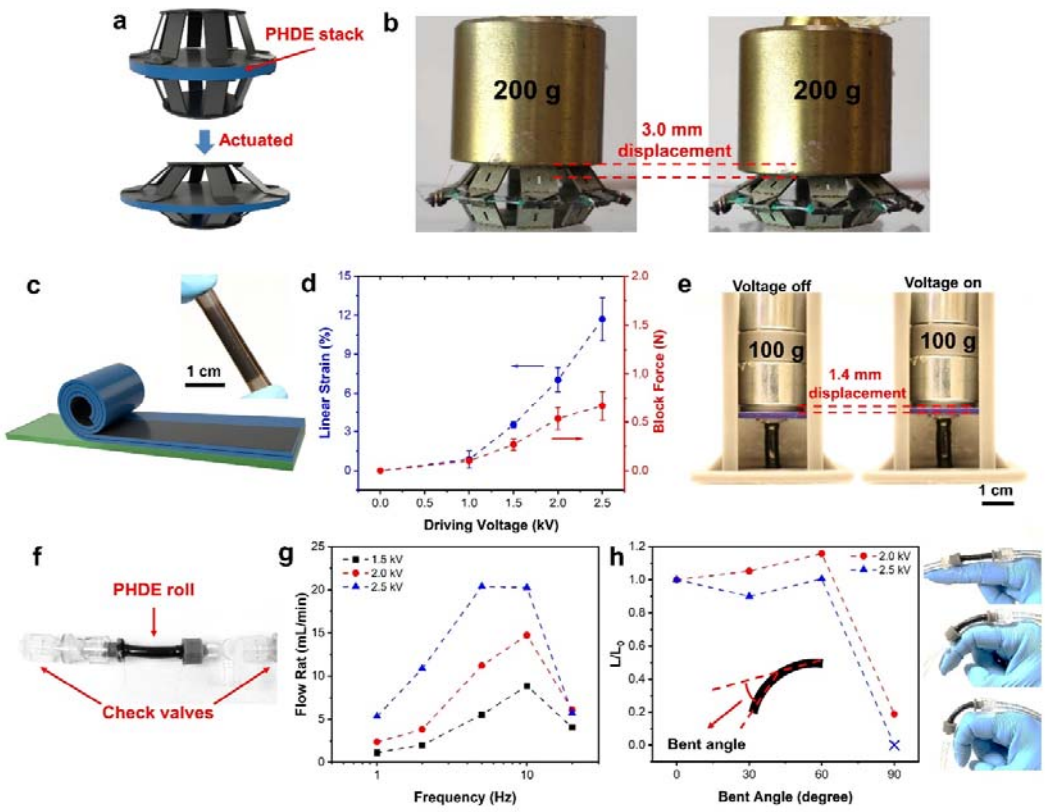

Fig. 4. New actuators enabled by multilayer PHDE. (a) Schematic illustrations of PHDE based spider actuators. (b) A PHDE spider actuator lifts a 200 g load at 2.5 kV. (c) Schematic illustration of fabrication of PHDE roll actuators. The inset shows the photo of a PHDE roll. (d) Linear strain and block force of PHDE roll actuators at different driving voltages. (e) A PHDE roll actuator lifts 100 g load at 0.5 Hz. (f) Photograph of a PHDE roll pump. (g) Water flow rates of a PHDE roll pump at different driving voltages and frequencies. (h) Normalized flow rates (L/L_0) at different bending angles. The driving frequency is 10 Hz. The photos to the right show a PHDE roll pump at different bending angles.

We also designed all-polymer multifunctional roll actuators using multilayer PHDE films. As shown in Fig. 4c, a 2-layer PHDE strip with 9 cm length was fabricated

on glass substrate via our “dry stacking” method. A binding layer was coated on the strip. The strip was then rolled into a free standing tube with an inner diameter of ~3 mm and an outer diameter of 5 mm. There are 11 rounds of the 2-layer stack in the roll, with inner-most and outer rounds acting as insulation, leading to a total of ~18 active layers in the roll. At 2.5 kV, the roll actuators generated a linear strain of ~11.7% with no load and a block force of ~0.70 N (~0.10 MPa stress) under a 0.5 N compressing pre-load (Fig. 4d). The operating voltage was lower than the 3.0 kV operating voltage for single layer flat films, because the PHDE films were slightly stretched during the rolling process. The actuation strain decreased with higher frequency, being ~8.1% at 2 Hz and ~4.1% at 20 Hz (Supplementary Fig. 18a). A PHDE roll actuator with 1 cm active length was tested to lift a 100 g load by 1.4 mm at 0.5 Hz, which translated to an output energy density of 15.6 J/kg based on the mass of the active material (Fig. 4e and Supplementary Movie 7). The displacement at 5 Hz was 1.1 mm (Supplementary Fig. 18b and Movie 7), with a power density calculated to be 122 W/kg. These values are lower than those determined in the pure-shear mode and the spider actuators. There are two main reasons for this. First, the presence of inactive layers in the rolled PHDE actuators constrain actuation to some degree. Second, the circumferential strain is not outcoupled resulting in effective energetic losses. However, the present roll is made entirely of polymers (except for a small amount of conductive materials), and it is compact and lightweight, without the use of any supporting structures which would add significant weight and volume[45,50]. Moreover, the PHDE rolls are highly robust and remain functional after they are bent, twisted, and hammered (Supplementary Fig. 19

and Movie 8).

To further utilize the circumferential strains of the all-polymer roll actuator, we developed a tubular pump with two check valves to help direct the flow direction (Fig. 4f). The flow rate (L) could be tuned by controlling the driving voltage and frequency. When used for pumping water, a PHDE roll pump with ~3 mm inner diameter reached a peak flow rate of ~20.4 mL/min at 2.5 kV, which translated to a specific flow rate of ~100,000 mL/min·kg (Fig. 4g and Supplementary Movie 9). This value is about two orders of magnitude higher than those of a high-performance miniature pump (TCS Micropumps, MGD 1000S) and a large off-the-shelf compressor (McMaster, single tank portable air compressor)[51]. Another unique feature of the PHDE roll pumps is their high flexibility. The flow rate even increased when the roll was bent up to 60 degree, possibly due to the small pre-strains incurred when they were bent (Fig. 4h). The falloff of the flow rate at 90 degree bending was caused by the flow passage getting partially blocked by the bent tube wall. The combined features of tunable flow rate, compactness, light weight, low noise, and high mechanical compliancy may find the PHDE roll pumps new applications in flexible medical implants and soft robotics.

In conclusion, a new dielectric elastomer (PHDE) has been synthesized with a bimodal network structure and their stress-strain relationship optimized by adjusting the concentration of the short-chain crosslinkers. A small amount of hydrogen bonds introduced into the elastomer network reduced the viscoelastic losses while maintaining the general stress-strain relationship. The resulting PHDE showed a maximum areal actuation strain of ~190% and fully suppressed EMI without an applied prestretching.

The PHDE also had fast response speed and achieved actuation strains over 110% at 2 Hz. The PHDE was further demonstrated to outcouple high force and work. A peak energy density of ~88 J/kg and power density of ~1970 W/kg were measured in pure-shear mode. The actuation properties allowed the demonstration of tossing a ball 20 times the weight of the PHDE film to a height of 16 times the diameter of the film and a jumping robot simply made of a PHDE film and a circular frame attached to three legs. Moreover, the processability of PHDE allowed a novel dry stacking method for fabrication of PHDE multilayer actuators. The 10-layer actuators were fabricated with performance similar to single layer actuators with strains over 110% at 2 Hz. These PHDE stacks were successfully used to build novel devices, such as spider actuators and multifunctional roll actuators with high actuation performance. The PHDE achieved actuation strains comparable to that of the best highly prestretched acrylic elastomers, with faster response, while embodying the processability afforded by silicone elastomers, without an applied prestretching.

The PHDE synthesis may open the door for rational design of new dielectric elastomers with mechanical and actuation properties tailored to meet specific application needs. The processability should allow integrated processes, involving microfabrication and 3D printing, which are necessary for the fabrication of insect-size robots, haptic and wearable devices and outperform natural muscle.

Methods

Materials

Urethane diacrylate (UDA, catalog name: CN9021) and isobornyl acrylate (IBOA) were obtained from Sartomer Company and used as received. Butyl acrylate (BA), acrylic acid (AA), neopentyl glycol propoxylate diacrylate (PNPDA), isopropyl alcohol (IPA), poly(acrylic acid) solution (M_w~ 100,000, 35 wt % in H_2O), benzophenone (BP) and 2,2-dimethoxy-2-phenylacetophenone (DMPA) were purchased from Sigma Aldrich and used as received. Single-walled carbon nanotubes (SWCNTs, catalog name: P3-SWNT) were purchased from Carbon Solutions, Inc.

Fabrication of single layer PHDE films for general testing

Each prepolymer solution was weighed out according to predetermined ratios and mixed overnight. To screen the formulation, the pre-polymer solution was spin coated onto a poly (acrylic acid) 5% solution (PAA) in IPA precoated glass substrate with 1000 rpm speed. The film thickness is dependent on the viscosity of pre-polymer solutions. PNPDA 5 samples have a thickness of ~35 μm, PNPDA 10 samples have a thickness of ~49 μm, and PNPDA 12 samples have a thickness of ~53 μm. The PAA coating acts as a sacrificial layer. The prepolymer solution coated on the glass was then UV cured in air on a UV curing conveyor equipped with 2.5 W/cm^2 Fusion 300s type "h" UV curing bulb for 2 passes at a speed of 6 ft/min. The glass with the film still coated on it was affixed to an acrylic frame (1/16 in thick, 0.8 in x 2.5 in opening) with double-sided tape. The outside of the glass was also taped to the frame and submerged in a water bath. After 1 hour, the film peeled off the glass and left to dry for at least 1 hour. Once completely dry, the film was coated (cotton swab) on both sides of the film with

a thin layer carbon grease (NyoGel 756G, Nye Lubricants) as compliant electrodes.

Fabrication of single layer PHDE films for multilayer actuators

Each prepolymer solution was weighed out according to wt% predetermined ratios and mixed overnight. The pre-polymer solution was then blade coated on a drawdown machine onto a glass substrate. The prepolymer solution coated on the glass was then UV cured in N_2 on a UV curing conveyor equipped with 2.5 W/cm^2 Fusion 300s type "h" UV curing bulb for 2 passes at a speed of 18 ft/min. The blade coated films have a uniform thickness of ~40 μm. For single layer testing with CNT electrode, the glass was still coated with PAA as sacrificial layer and then with the film was affixed to an acrylic frame (1/16 in thick, 0.8 in x 2.5 in opening) with double-sided tape. The outside of the glass was also taped to the frame and submerged in a water bath. After 1 hour, the film was peeled off the glass and left to dry for at least 1 hour. Once completely dry, the film was sprayed at 30 psi with a CNT solution as the compliant electrode. For single layer films used in the multilayer actuator, CNTs are spray coated onto glass/DE films with paper masks to form patterned electrodes. The conductivity of CNT electrodes is ~100 kΩ/square, which is controlled by the amount of solution sprayed per film. After the electrodes are patterned, the paper masks are removed, and the films are sprayed with diluted DE monomer solutions as a binding layer.

The CNT solution is prepared by mixing 5 mg CNT with 2 mL DI water and 20 mL IPA.

Fabrication of multilayer PHDE actuators

DE films are prepared on glass slides and 170 μm thick PET slides via blade coating and in situ UV curing. The films are trimmed to ensure DE film thickness uniformity. The PET/DE film is aligned onto glass/DE film and placed in the chamber of laminator. The laminating machine vacuums the chamber and laminates the sample with a pressure of 2 kg/cm^2. The stack is placed under UV irradiation in air to cure the binding layer. After UV curing, the stack is heated on a hot plate at 80°C for 1 min. The PET together with stacked DE films are peeled off from the glass substrate. The process is then repeated for each proceeding layer until the desired number of layers is achieved.

Fabrication of spider actuators

Spider actuators were assembled using *Smart Composite Microstructures*, a laminate composite fabrication approach previously employed to build insect-inspired robots[52]. The mechanisms are comprised of rigid materials (fiber-reinforced plastics, or even paper), cut with a laser, and laminated as a sandwich construction with a polymer flexure (typically polymide). Four-layer DE stacks were fabricated with a 1-inch diameter active area, reinforced around the edge with 3M Fastbond contact adhesive to increase tear resistance and trimmed with a laser cut. The laminate flexures were cut separately and attached to the film using an alignment jig.

Fabrication of multifunctional roll actuators

The fabrication of the rolled actuators begin with the assembly of a two layer actuator.

First, ~2 g PHDE was deposited onto a 4” by 5” glass slide. It was then blade coated at a speed of 1 inch per second to yield a 40 μm film. The PHDE film was cured in a nitrogen environment under UV light. Next, 0.5 mL of a 5 wt% PAA/IPA solution was deposited, and blade coated onto a 4” by 5” Kapton substrate. The blade coater had a 0.0005” gap. The PAA sacrificial layer was allowed to dry for 20 minutes at room temperature. The PHDE casting and curing process was then repeated over the sacrificial layer.

To pattern the electrodes, 8 mL CNT solutions were deposited via spray deposition onto the Glass/PHDE substrate through a contact mask. Each roll was comprised of a 10 cm by 1 cm film with an active length of 9 cm and an active width of 1 cm. For the pump demonstration, rolls with 9 cm by 2 cm active areas were fabricated. 10 mL of diluted DE monomer solutions, which acted as a binding layer, was deposited via spray deposition. The Glass/PHDE substrate was aligned and cured to the PHDE/PAA/Kapton substrate. The bonded structure was then soaked in DI water for 30 minutes to dissolve the sacrificial PAA layer. The Kapton film was then gently peeled away, and the resulting multilayer actuator on glass was allowed to dry at room temperature overnight. The outer CNT electrode was deposited in the same manner as the inner electrode. An outer binding layer was also deposited.

In order to roll the 2-layer actuators, 1/8 inch diameter steel dowels were first wrapped with parchment paper to provide a nonstick surface. Then at 60 ˚C, the 2-layer actuators were slowly rolled onto the parchment-lined dowel ensuring no wrinkles or bubbles formed during the rolling process. After the rolling process was completed, the

PHDE roll with ~20 layers was slipped off the parchment-lined steel dowel and cured under UV light. The ends of the roll were cut to expose the inner electrodes. Carbon grease was smeared on the ends to make electrical contact to the inner electrodes.

The rolled actuators were then incorporated into the pump demonstration using custom 3D-printed luer-lock barb adapters with integrated electrical contacts. The luer-locks allow for a water and air-tight connection to the rest of the fluidic system. Single check valves were placed upstream and downstream from the roll to control flow of the pump. After the fluidic system was primed with a syringe via a three-way stopcock, it could be operated at a variety of frequencies, voltages, and operating angles.

Energy and power density measurements of PHDE films in pure-shear mode

PHDE single layer films or 10-layer stacks with 6 cm by 1 cm active area were fabricated and 170 μm thick PET strips with 0.5 cm width were adhered on top and bottom edges of PHDE films with 3M Fastbond to constrain the active films. The samples were tested under isotonic conditions by hanging specific masses at the bottom. Voltages were applied across the film and the actuation strain during contraction of PHDE films were recorded by a digital camera. As the maximum linear strain in these measurements was less than 80% and the stress-strain relationship of PHDE within this strain range was close to linear, the energy and power output of PHDE were calculated based on the potential energy increase of the hanging mass during contraction of the PHDE films.

Permittivity measurement

Elastomer materials of known thickness were coated in carbon grease to form circular electrodes with diameter 0.3 inches. Capacitance was measured using GwInstek LCR-819 LCR meter at 1 V excitation and 12 to 1,000 Hz frequency. Relative permittivity ε was calculated by:

$$\varepsilon = Cz/\varepsilon_0 A \qquad \text{Eq. 4}$$

Where C is the measured capacitance, z is the thickness of the elastomer film, ε_0 is the vacuum permittivity, and A is the effective area.

Actuation tests

The electrode coated elastomer films were attached to a diaphragm chamber made of aluminum with a 0.84 cm (0.33 inch) circular opening onto with the DE films were attached. A positive air pressure (~0.33 kPa) was applied in the chamber such that when the films were actuated, they would deform out of plane to form a raised dome. The active area of the DE films was flat and circular with a diameter of 0.76 cm (0.3 inch), before actuation. A high voltage supply was used to drive the actuation. A digital camera was used to record the actuation of the DE films. The actuation strain was measured from the video frame-by-frame through MATLAB image processing tools and calculated using an equation for the surface area of a dome.

$$s_A = \frac{(h^2+R^2)-(h_0^2+R_0^2)}{(h_0^2+R_0^2)} \qquad \text{Eq. 5}$$

Where h is the height of the dome and R is the radius. The strain values at each voltage were calculated after a constant driving voltage at 0.1 Hz. The frequency of the voltage

was then increased to 0.5 Hz up to 10 Hz. The nominal electric field was calculated by dividing the applied voltage by the initial thickness of the elastomer film at maximum strain. At least three samples were tested for each formulation.

Dynamic mechanical analysis

Mechanical properties were measured on a TA Instruments RSAIII dynamic mechanical analyzer (DMA). Dynamic temperature sweep tests were conducted at a temperature ramping rate of 2 °C/min and a frequency of 1 Hz from -50 to 100 °C with samples of 8 mm wide and 50 μm thick loaded onto the DMA with a 10 mm gap between the thin film grips. The maximum elongation strain of the samples were obtained at room temperature with a stretching rate of 0.5 mm/s. The tested samples used were 8 mm wide and 50 μm thick with a 6 mm gap between the thin film grips of the DMA. Samples were measured in triplicate at least.

Data availability

The data that support the findings of this study are available from the corresponding authors upon request.

References

1. Pelrine, R., Kornbluh, R., Pei, Q. & Joseph, J. High-Speed Electrically Actuated Elastomers with Strain Greater Than 100%. *Science* **287**, 836-839 (2000).

2. Pelrine, R., Pei, Q. & Kornbluh, R. Dielectric elastomers: past, present, and potential future. *Proc. SPIE 10594, Electroactive Polymer Actuators and Devices (EAPAD) XX*, 1059406 (2018).

3. Shankar, R., Ghosh, T. K. & Spontak, R. J. Dielectric elastomers as next-generation polymeric actuators. *Soft Matter* **3**, 1116-1129 (2007).

4. Qiu, Y., Zhang, E., Plamthottam, R. & Pei, Q. Dielectric Elastomer Artificial Muscle: Materials Innovations and Device Explorations. *Acc. Chem. Res.* **52**, 316-325 (2019).

5. O'Halloran, A., O'Malley, F. & McHugh, P. A review on dielectric elastomer actuators, technology, applications, and challenges. *J. Appl. Phys.* **104**, 071101 (2008).

6. Duduta, M., Hajiesmaili, E., Zhao, H., Wood, R. J. & Clarke, D. R. Realizing the potential of dielectric elastomer artificial muscles. *Proc. Natl. Acad. Sci. USA* **116**, 2476-2481 (2019).

7. Chen, Y. *et al.*, Controlled flight of a microrobot powered by soft artificial muscles. *Nature* **575**, 324-329 (2019).

8. Ji, X. *et al.*, An autonomous untethered fast soft robotic insect driven by low-voltage dielectric elastomer actuators. *Sci. Robot.* **4**, eaaz6451 (2019).

9. Anderson, I. A., Gisby, T. A., McKay, T. G., O'Brien, B. M. & Calius, E. P. Multi-functional dielectric elastomer artificial muscles for soft and smart machines. *J. Appl. Phys.* **112**, 041101 (2012).

10. Suo, Z. Theory of dielectric elastomers. *Acta Mech. Solida Sin.* **23**, 549-578 (2010).

11. Romasanta, L. J., Lopez-Manchado, M. A. & Verdejo, R. Increasing the performance of dielectric elastomer actuators: A review from the materials perspective. *Prog. Polym. Sci.* **51**, 188-211 (2015).

12. Bar-Cohen, Y. & Anderson, I. A. Electroactive polymer (EAP) actuators—background review. *Mech. Soft Mater.* **1**, 5 (2019).

13. Brochu, P. & Pei, Q. Advances in Dielectric Elastomers for Actuators and Artificial Muscles. *Macromol. Rapid Commun.* **31**, 10-36 (2010).

14. Shit, S. C. & Shah, P. A Review on Silicone Rubber. *Nat. Acad. Sci. Lett.* **36**, 355-365 (2013).

15. Rosset, S., Poulin, A., Shea, H. & Anderson, I. Taming the viscoelastic creep of dielectric elastomer actuators. *Proc. SPIE 10966, Electroactive Polymer Actuators and Devices (EAPAD) XXI*, 1096614 (2019).

16. Vatankhah-Varnoosfaderani, M. *et al.*, Bottlebrush Elastomers: A New Platform for Freestanding Electroactuation. *Adv. Mater.* **29**, 1604209 (2017).

17. Zhao, X. & Suo, Z. Theory of Dielectric Elastomers Capable of Giant Deformation of Actuation. *Phys. Rev. Lett.* **104**, 178302 (2010).

18. Niu, X. *et al.*, Synthesizing a new dielectric elastomer exhibiting large actuation strain and suppressed electromechanical instability without prestretching. *J. Polym. Sci. B Polym. Phys.* **51**, 197-206 (2013).

19. Plante, J. S. & Dubowsky, S. On the properties of dielectric elastomer actuators and their design implications. *Smart Mater. Struct.* **16**, S227-S236 (2007).

20. Jiang, L., Betts, A., Kennedy, D. & Jerrams, S. Eliminating electromechanical instability in dielectric elastomers by employing pre-stretch. *J. Phys. D Appl. Phys.* **49**, 265401 (2016).

21. Duduta, M., Wood, R. J. & Clarke, D. R. Multilayer Dielectric Elastomers for Fast, Programmable Actuation without Prestretch. *Adv. Mater.* **28**, 8058-8063 (2016).

22. Rosset, S. & Shea, H. R. Small, fast, and tough: Shrinking down integrated elastomer transducers. *Appl. Phys. Rev.* **3**, 031105 (2016).

23. Kovacs, G., Düring, L., Michel, S. & Terrasi, G. Stacked dielectric elastomer actuator for tensile force transmission. *Sens. Actuator A Phys.* **155**, 299-307 (2009).

24. Kovacs, G. & Düring, L. Contractive tension force stack actuator based on soft dielectric EAP. *Proc. SPIE 7287, Electroactive Polymer Actuators and Devices (EAPAD) 2009*, 72870A (2009).

25. Behboodi, A. & Lee, S. C. K. in *2019 IEEE 16th International Conference on Rehabilitation Robotics (ICORR)*. 499-505 (2019).

26. Daniel, W. F. M. *et al.*, Solvent-free, supersoft and superelastic bottlebrush melts and networks. *Nat. Mater.* **15**, 183-189 (2016).

27. Ha, S. M., Yuan, W., Pei, Q., Pelrine, R. & Stanford, S. Interpenetrating Polymer Networks for High-Performance Electroelastomer Artificial Muscles. *Adv. Mater.* **18**, 887-891 (2006).

28. Ha, S. M. *et al.*, High electromechanical performance of electroelastomers based on interpenetrating polymer networks. *Proc. SPIE 6927, Electroactive Polymer Actuators and Devices (EAPAD) 2008*, 69272C (2008).

29. Brochu, P., Stoyanov, H., Niu, X. & Pei, Q. All-silicone prestrain-locked interpenetrating polymer network elastomers: free-standing silicone artificial muscles with improved performance and robustness. *Smart Mater. Struct.* **22**, 055022 (2013).

30. Ellingford, C., Bowen, C., McNally, T. & Wan, C. Intrinsically Tuning the Electromechanical Properties of Elastomeric Dielectrics: A Chemistry Perspective. *Macromol. Rapid Commun.* **39**, 1800340 (2018).

31. Opris, D. M. *et al.*, New Silicone Composites for Dielectric Elastomer Actuator Applications In Competition with Acrylic Foil. *Adv. Funct. Mater.* **21**, 3531-3539 (2011).

32. Caspari, P., Dünki, S. J., Nüesch, F. A. & Opris, D. M. Dielectric elastomer actuators with increased dielectric permittivity and low leakage current capable of suppressing electromechanical instability. *J. Mater. Chem. C* **6**, 2043-2053, (2018).

33. Sheima, Y., Caspari, P. & Opris, D. M. Artificial Muscles: Dielectric Elastomers Responsive to Low Voltages. *Macromol. Rapid Commun.* **40**, 1900205, (2019).

34. Opris, D. M. Polar Elastomers as Novel Materials for Electromechanical Actuator Applications. *Adv. Mater.* **30**, 1703678, (2018).

35. Tugui, C. *et al.*, Bimodal silicone interpenetrating networks sequentially built as electroactive dielectric elastomers. *J. Mater. Chem. C* **3**, 8963-8969 (2015).

36. Rubinstein, M., & Panyukov, S. Elasticity of Polymer Networks. *Macromolecules* **35**, 6670-6686 (2002).

37. Carpi, F. *et al.*, Standards for dielectric elastomer transducers. *Smart Mater. Struct.* **24**, 105025 (2015).

38. Zhang, L. *et al.*, A highly stretchable, transparent, notch-insensitive self-healing elastomer for coating. *J. Mater. Chem. C* **8**, 2043-2053 (2020).

39. Mathis, L., Chen, Y. & Shull, K. R. Tuning the Viscoelasticity of Hydrogen-Bonded Polymeric Materials through Solvent Composition. Macromolecules 51, 3975-3982, doi:10.1021/acs.macromol.8b00344 (2018).

40. Guo, H., Han, Y., Zhao, W., Yang, J. & Zhang, L. Universally autonomous self-healing elastomer with high stretchability. *Nat. Commun.* **11**, 2037 (2020).

41. Lewis, C. L., Stewart, K. & Anthamatten, M. The Influence of Hydrogen Bonding Side-Groups on Viscoelastic Behavior of Linear and Network Polymers. *Macromolecules* **47**, 729-740 (2014).

42. Koh, S. J. A. *et al.* High-performance electromechanical transduction using

laterally-constrained dielectric elastomers part I: Actuation processes. *J. Mech. Phys. Solids* **105**, 81-94, (2017).

43. Acome, E. *et al.* Hydraulically amplified self-healing electrostatic actuators with muscle-like performance. *Science* **359**, 61-65, (2018).

44. Stoyanov, H., Brochu, P., Niu, X., Gaspera, E. D. & Pei, Q. Dielectric elastomer transducers with enhanced force output and work density. *Appl. Phys. Lett.* **100**, 262902, (2012).

45. Hau, S., Rizzello, G. & Seelecke, S. A novel dielectric elastomer membrane actuator concept for high-force applications. *Extreme Mech. Lett.* **23**, 24-28, (2018).

46. Cao, C. *et al.* Uncovering isolated resonant responses in antagonistic pure-shear dielectric elastomer actuators. *Soft Sci.* **1**, 1, (2021).

47. Rich, S. I., Wood, R. J. & Majidi, C. Untethered soft robotics. *Nat. Electron.* **1**, 102-112, (2018).

48. Araromi, O. A. *et al.*, Spray deposited multilayered dielectric elastomer actuators. *Sens. Actuator A Phys.* **167**, 459-467 (2011).

49. Pelrine, R. *et al.* Applications of dielectric elastomer actuators. *Proc. SPIE 4329, Smart Structures and Materials 2001: Electroactive Polymer Actuators and Devices* (2001).

50. Pei, Q., Rosenthal, M., Pelrine, R., Stanford, S. & Kornbluh, R. Multifunctional electroelastomer roll actuators and their application for biomimetic walking robots. *Proc. SPIE 4698, Smart Structures and Materials*

2002: Industrial and Commercial Applications of Smart Structures Technologies, (2002).

51. Cacucciolo, V. *et al.* Stretchable pumps for soft machines. *Nature* **572**, 516-519, (2019).

52. Wood, R. J. The First Takeoff of a Biologically Inspired At-Scale Robotic Insect. *IEEE Trans. Robot.* **24**, 341-347, (2008).

Acknowledgements

We would like to acknowledge Roy Kornbluh of SRI International for valuable suggestions in designing the ball tossing and jumping robot experiments. We acknowledge financial support from the Defense Advanced Research Projects Agency (DARPA) (Contract # HR001119C0043).

.

Author information

Affiliations

Department of Materials Science and Engineering, University of California, Los Angeles, Los Angeles, CA, USA

Ye Shi, Erin Askounis, Roshan Plamthottam, Zihang Peng, Kareem Youssef, Junhong Pu & Qibing Pei

SRI International, Menlo Park, CA, USA

Tom Libby, Ron Pelrine

Current address: Pelrine Innovations LLC, Boulder, CO, USA

Ron Pelrine

Contributions

Y. S., E. A. and R. Pl. contributed equally to this work. Y. S., E. A., R. Pl. and Q. P. conceived the idea. E. A., Y. S. and R. Pl. performed materials synthesis, characterizations and thin film preparation. Y. S. and R. Pl. performed device fabrication and characterizations including multilayer stacks, planar jumping robots, and roll actuators. T. L. fabricated and tested spider actuators. K. Y., Z. P. and J. P. helped on film fabrication and material characterizations. Q. P. directed the project. Y. S., E. A., R. Pl., R. Pe., T. L. and Q. P. designed the actuators, analyzed the data, discussed the results, and wrote the manuscript.

Corresponding authors

Correspondence to Qibing Pei.

Ethics declarations

Competing interests

Q. P., E. A. and Y. S. are applying for patents related to the described work. The other authors declare that they have no competing interests.

Supplementary information

Supplementary Information

Supplementary Movie S1 to Movie S9